Enhanced sodium-ion storage capability of P2/O3 biphase by Li-ion substitution into P2-type $Na_{0.5}Fe_{0.5}Mn_{0.5}O_2$ layered cathode

Ganesh Kumar Veerasubramani [a], Yuvaraj Subramanian [a], Myung-Soo Park [a],
Baskar Senthilkumar [b], Ali Eftekhari [c], Sang Jae Kim [d], Dong-Won Kim [a, *]

[a] Department of Chemical Engineering, Hanyang University, Seoul, 04763, South Korea
[b] Materials Research Center, Indian Institute of Science, C.V. Raman Avenue, Bangalore, India
[c] Belfast Academy, 2 Queens Road, Belfast, BT3 9FG, United Kingdom
[d] Department of Mechatronics Engineering, Jeju National University, Jeju 63243, South Korea

ARTICLE INFO

ABSTRACT

Integration of P2 and O3 phases in $Na_{0.5}Fe_{0.5}Mn_{0.5}O_2$ cathode via Li-ion substitution is proposed to enhance its electrochemical performance for sodium-ion battery applications. The formation of P2 and the combination of P2/O3 intergrowth were confirmed by X-ray diffraction refinement, high resolution transmission electron microscopy and X-ray photoelectron microscopy analyses. Various content of lithium was used to find optimum P2+O3 combinations. The optimized Li-ion substituted $Na_{0.5}(Li_{0.10}Fe_{0.45}Mn_{0.45})O_2$ showed a high initial discharge capacity of 146.2 mAh g^{-1} with improved cycling stability, whereas the pristine $Na_{0.5}Fe_{0.5}Mn_{0.5}O_2$ initially delivered a discharge capacity of 127.0 mAh g^{-1}. In addition, the combination of P2+O3 increased its average voltage, which is important for achieving high energy density sodium-ion batteries. Overall, the prepared $Na_{0.5}(Li_{0.10}Fe_{0.45}Mn_{0.45})O_2$ electrode exhibited the improved cycling performance in terms of reversible capacity and rate capability compared to pristine $Na_{0.5}Fe_{0.5}Mn_{0.5}O_2$ electrode material.

© 2018 Elsevier Ltd. All rights reserved.

1. Introduction

In these days, with a raising demand on energy worldwide because of the exhaustion of fossil fuels, the development of substitute energy conversion and storage systems is required for the advancement of mankind in various fields such as residential, industry, transportation, space exploration and military [1]. Over the past few decades, the development of lithium-ion batteries (LIBs) emerged rapidly due to urgent demand for developing sustainable energy storage systems for various electronic devices such as portable laptops, smartphones and so on; because of their high energy density and excellent cycle life [2—4]. However, to meet the essential demand of advanced power sources such as electric vehicles and large-scale energy storage systems, further development in the storage ability is required [5]. Among the various rechargeable battery systems, sodium-ion battery (SIB) is one of the promising candidates due to its low cost for large-capacity energy storage applications [6—10]. Numerous attempts have been made

so far to develop more practical cathode materials for sodium-ion batteries. Sodium-based layered oxide Na_xMO_2 materials (M = 3d transition metal) have received much attention due to their reversible behaviour and large specific capacity. Such layered oxide materials can be classified into two types; P2 and O3, in which sodium layers are accommodated with the M layers in prismatic and octahedral structure, respectively [11—15]. The P2 phase sustains during sodium de-intercalation process due to its direct sodium ion diffusion and has a more open pathway. However, the structural changes are occurred by over-extraction of sodium ions at higher potential, which restricts the reversible charge and discharge cycles [16—23]. In contrast, O3 phase acting as sodium ion accumulator can furnish sufficient amount of sodium ions during the electrochemical reaction. However, the intrusion of intermediate tetrahedral sites during sodium ion migration requires to overcome the high energy obstacle for O3 type structure, the ineluctable phase transition affecting the electrochemical reaction, and sluggish kinetics [16,24—26].

To solve these issues, utilizing the advantages of both phases can be a practical strategy to prepare the high-performance cathode materials for sodium-ion batteries. Recently, the combination of

* Corresponding author.
  E-mail address: dongwonkim@hanyang.ac.kr (D.-W. Kim).

two phases in a single material by substituting cations has drawn considerable attention due to its excellent electrochemical performance as compared to the single structured electrode material [27–33]. For example, Guo et al. reported the biphasic $Na_{0.66}Li_{0.18}Mn_{0.71}Ni_{0.21}Co_{0.08}O_{2+\delta}$ to deliver a high discharge capacity of 200 mAh g^{-1} at 0.1 C rate and achieved the stable cycling behaviour [28]. Li et al. reported that the P2 and O3 biphasic $Na_{2/3}Mn_{0.55}Ni_{0.25}Ti_{0.2-x}Li_xO_2$ exhibited a discharge capacity of 158 mAh g^{-1} at 12 mA g^{-1}, which was higher than Li-free cathode material (147 mAh g^{-1}) [30]. More recently, Qi et al. reported the hybrid structure of $Na_{0.78}Ni_{0.2}Fe_{0.38}Mn_{0.42}O_2$ could deliver a discharge capacity of 86 mAh g^{-1} with excellent high rate performance [32]. Kwon et al. reported the $Na_{0.7}[Mn_{1-x}Li_x]O_{2+y}$ had an excellent cycling stability than the pristine $Na_{0.7}MnO_{2+y}$, even though the pristine material showed a higher capacity [33]. However, very limited studies have been reported so far based on the combination of two phases in the cathode material of sodium-ion batteries. There are various types of synthesis techniques available for preparing the layered cathodes [34,35]. Among them, sol−gel technique provides many advantages, particularly, it is able to synthesize the solid-state material from the chemically homogeneous precursor. There is a possibility to produce complex inorganic and other nanomaterials even at shorter preparation times and lower preparation temperatures by snaring the randomness of the solution of chemicals and reagents [35,36]. In addition, sol−gel chemistry can control the morphology and size of the products. By considering all the above aspects, in this work, we report the combination of the P2 and O3 phases of lithium-ion substituted $Na_{0.5}[Li_x(Fe_{0.5}Mn_{0.5})_{1-x}]O_2$ (LNFMO) as a promising cathode for sodium-ion battery applications by sol-gel technique, which delivers a specific capacity of 146.2 mAh g^{-1} with enhanced cyclic stability, average voltage, coulombic efficiency and rate capability compared to the single phase P2 structured $Na_{0.5}Fe_{0.5}Mn_{0.5}O_2$ (NFMO) material.

2. Experimental

2.1. Materials synthesis

Layered LNFMO materials were synthesized by sol-gel technique, as schematically presented in Fig. 1. The starting precursor materials (acetates of Li, Na, Fe and Mn) and citric acid were mixed, and the mixture was kept with stirring at 80 °C for 12 h. Then, temperature was increased to 120 °C to form the xerogel. Finally, the obtained powder was heated to 400 °C for 5 h and followed by 900 °C for 12 h to obtain $Na_{0.5}[Li_x(Fe_{0.5}Mn_{0.5})_{1-x}]O_2$. The same procedure was followed to prepare pristine NFMO material without the addition of Li source. In this work, the amount of lithium was varied to find out the optimum combination of P2+O3 phase in $Na_{0.5}[Li_x(Fe_{0.5}Mn_{0.5})_{1-x}]O_2$. For simplicity, the pristine $Na_{0.5}Fe_{0.5}Mn_{0.5}O_2$ was denoted as NFMO, whereas Li-substituted $Na_{0.5}[Li_x(Fe_{0.5}Mn_{0.5})_{1-x}]O_2$ was expressed as LNFMO-n. That is, LNFMO-5 for x = 0.05, LNFMO-10 for x = 0.10 and LNFMO-20 for x = 0.20.

2.2. Electrode preparation and cell assembly

The electrode slurry was prepared by mixing 70 wt% active materials (LNMFO-n or NFMO) with 20 wt% Super-P and 10 wt% poly(vinylidene fluoride) binder in N-methyl pyrrolidine. The electrode was prepared by coating the slurry onto the Al foil and drying in a vacuum oven at 110 °C for 12 h. The active mass loading in the electrode was about 2.5 mg cm^{-2}. In order to evaluate the electrochemical performance of the LNMFO-n electrodes, a CR2032-type coin cell was assembled by sandwiching a glass fiber separator (Whatman CAT No. 1823-047) between sodium foil (Alfa Aesar 99%) and LNMFO-n electrode. A liquid electrolyte consisting of 1.0 M $NaClO_4$ in ethylene carbonate (EC)/propylene carbonate (PC) (50:50 by volume, battery grade) containing 5.0 wt% fluoroethylene carbonate (FEC) as an additive was kindly supplied by PANAX ETEC Co. Ltd. and was used as received. Karl Fisher titration using Mettler-Toledo Coulometer confirmed that the water content in the liquid electrolyte was less than 20 ppm. All the cells were assembled in glove box under argon atmosphere.

2.3. Characterization and measurements

Crystal structure was identified by powder X-ray diffraction (XRD). The XRD patterns were collected on an X-ray diffractometer (D8 Bruker) with Cu Kα radiation (λ = 1.5405 Å). Rietveld refinement of XRD pattern was performed by General Structure Analysis System (GSAS) in order to get the detailed structural information. The morphologies of the prepared samples were investigated by scanning electron microscope (NOVA Nano SEM-450) equipped
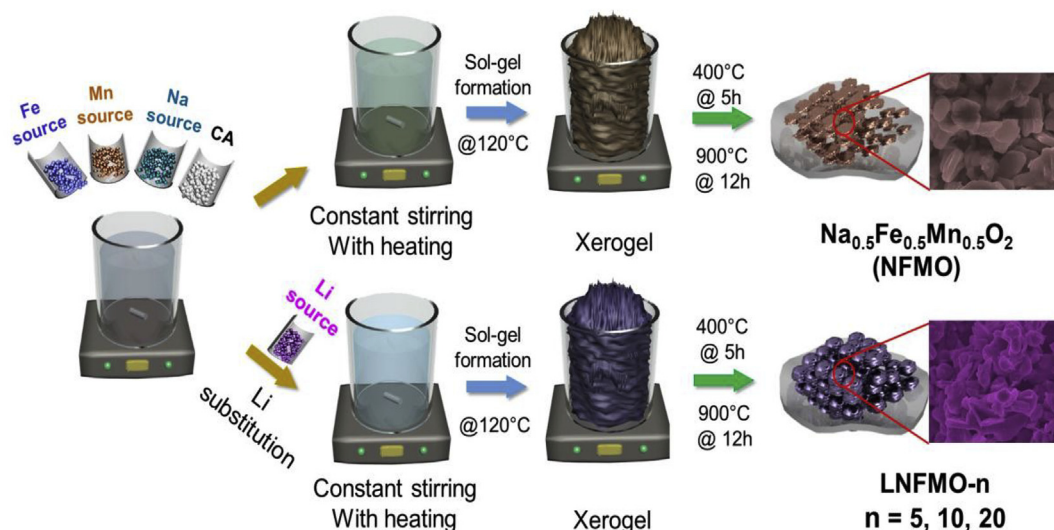

Fig. 1. Schematic illustration of the synthesis of pristine NFMO and LNFMO-n cathode materials by sol-gel technique.

with energy dispersive spectroscopy (EDS). The stoichiometric composition of each element in the prepared samples was determined with inductively coupled plasma-optical emission spectrometry (ICP-OES, Perkin Elmer, OPTIMA 8300). A high-resolution transmission electron microscope (HRTEM, JEOL, JEM 2100F) was used to observe the morphology of the prepared materials. The X-ray photoelectron spectroscopy (XPS) was conducted with a spectrometer having Mg/Al Kα radiation (XPS, VG Multilab ESCA System, 220i). Cyclic voltammetry (CV) was carried out in the potential range of 1.5–4.0 V with counter and reference electrodes of sodium metal, at a scan rate of 0.1 mV s^{-1} using CHI660D electrochemical workstation. Cycling test was conducted at a constant current density using battery testing equipment (WBCS 3000, Wonatech) at 25 °C.

3. Results and discussion

Fig. S1 shows the XRD patterns of NFMO and LNFMO-n materials containing different amounts of lithium. Rietveld refinement of XRD data along with that of the pristine sample was investigated in order to determine the unit cell parameters, and the detailed XRD refinement results are summarized in the Supplementary Materials. The crystalline peaks for pristine NFMO can be indexed as a hexagonal lattice with the space group $P6_3/mmc$, which are corresponding to the characteristic peak of P2-type, as depicted in Fig. 2(a). It shows the purity of the P2 structure with space group $P63/mmc$ and the lattice parameters are refined to be a = b = 2.92290 Å, c = 11.27188 Å, and V = 83.397913 Å^3 (Detailed crystallographic data on refined P2-type are listed in Tables S1 and S2). When substituting lithium into NFMO, O3 layered structure was formed by diminishing the peak intensity of P2 structure, as illustrated in Fig. 2(b) and Fig. S1, with slight peak shift and new peaks at 37.0, 41.7, 44.8, 52.5 and 56.9° corresponding to the O3 phase with the space group of R-3m. The crystalline peaks of LNFMO-10 are well matched to the standard ICSD card no: 252025 for the O3-phase with the trigonal structure and ICSD card no: 251549 for P2-phase with hexagonal lattice. From the Rietveld refinement of LNFMO-10, the calculated P2/O3 phase ratio was 32/68. Here, P2 phase was fitted for lattice parameters of a = b = 2.91532 Å, c = 11.15800 Å, and V = 82.127656 Å^3, and O3 phase was refined as lattice parameters of a = b = 2.92010 Å, c = 16.79270 Å, and V = 124.007113 Å^3. The detailed refinement results of LNFMO-10 were shown in Tables S3–S6. Note that the major difference is observed between c = 11.27188 Å for NFMO and c = 11.15800 Å for LNFMO-10, suggesting that the Li-ion is mainly entered into transition metal sites and certain amounts of Li-ions occupy the Na sites, which is consistent with the previous reports [27,30,38]. When Li content was higher than 0.1, the O3 phase was dominant compared to P2. Crystal structure of P2 and O3 phases are represented in Fig. 2(c). The crystal structure of P2 consists of ordered layered and stacked MO$_2$ (M = Fe and Mn) and Na layers [12,37]. The prismatic P2 can be denoted because Na$^+$ occupies two different sites between two prismatic AB-BA layers. In O3 phase, there is only one occupancy site for Na$^+$ that shares all the six edges with octahedrons of transition metal layers [39]. Hence, the diffusion of Na$^+$ ions has to surpass the smaller tetrahedron sites, and this limits ionic conductivity and rate performance. In contrast, the sodium layers sit between two different sites in P2 phase. Thus, there is an open pathway along with the face shared triangular prism, resulting in the improvement of rate performance [40]. Accordingly, the presence of O3 phase with good structural stability is anticipated to have the positive impact on retaining the P2 phase during electrochemical process. Molar ratio of each element in the NFMO and LNFMO-10 samples was determined by ICP-OES analysis, and the results are summarized in Table S7. According to ICP-
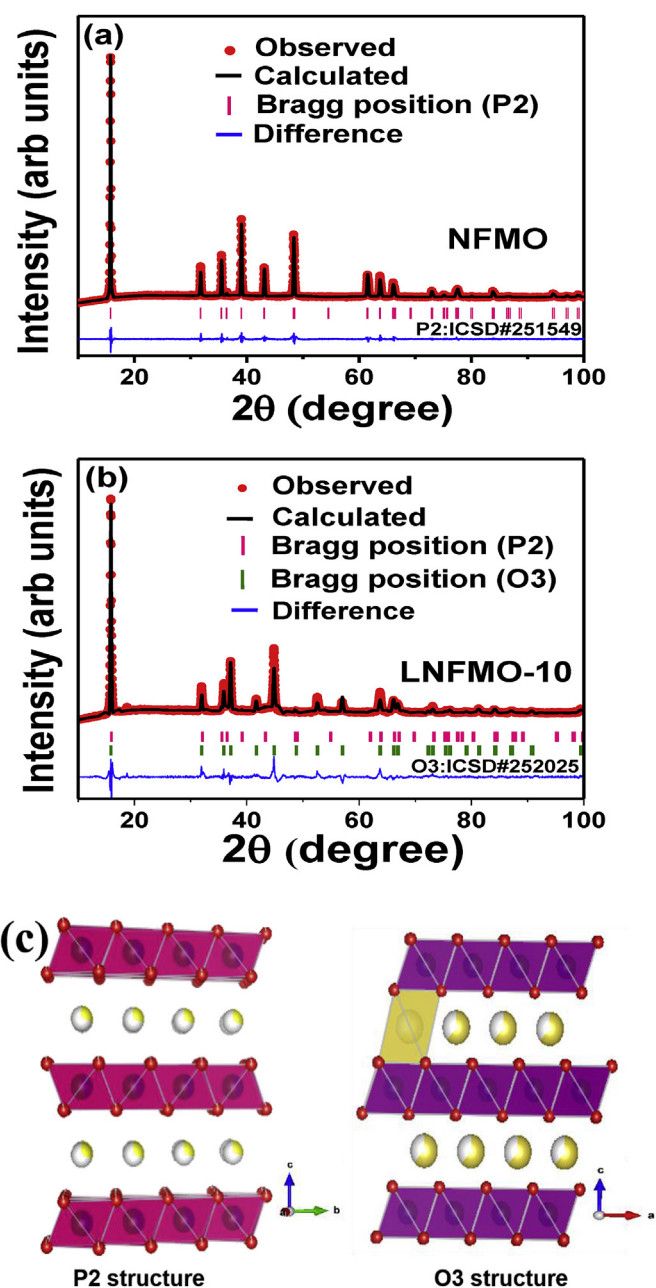

Fig. 2. XRD refinement patterns of (a) pristine NFMO and (b) LNFMO-10 materials. (c) P2 and O3 crystal structure; yellow, red and blue atoms correspond to sodium, oxygen and transition metal, respectively. (For interpretation of the references to colour in this figure legend, the reader is referred to the Web version of this article.)

OES results, the molar composition of each element in the obtained samples are in close agreement with stoichiometric atomic ratio in the samples.

The oxidation state of the cathode materials under consideration was investigated using XPS spectra (Fig. S2 and Fig. 3). The Li1s core-level spectrum in Fig. 3(a) shows only one peak at 54.7 eV. Na1s core-level spectrum of pristine NFMO exhibits only one peak at 1070.7 eV (Fig. S2(a)). In case of LNFMO-10, Na1s peak resides in almost same energy (1070.8 eV) like NFMO, as shown in Fig. 3(b). Two major peaks were observed at 711.7 and 725.6 eV in the Fe2p core-level spectrum of pristine NFMO (Fig. S2(b)), which could be assigned to Fe2p$_{3/2}$ and Fe2p$_{1/2}$, respectively. Very small shifts in binding energies (712.0 and 726.1 eV) for LNFMO-10 (Fig. 3(c)) were
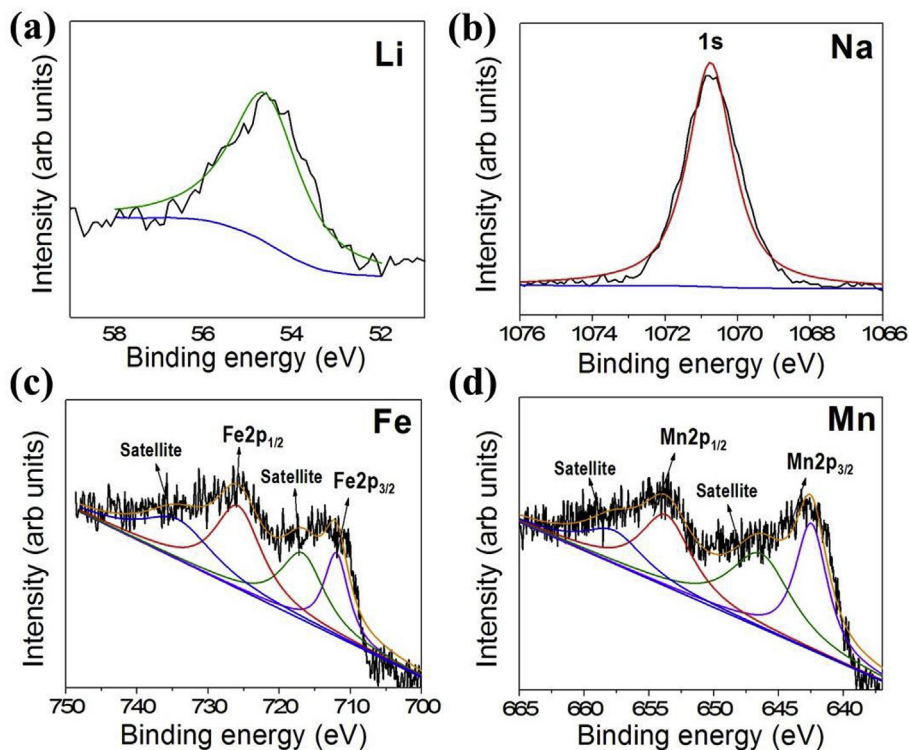
Fig. 3. XPS spectra of (a) Li1s core-level, (b) Na1s core-level, (c) Fe2p core-level and (d) Mn2p core-level of LNFMO-10 material.

observed, indicating stable oxidation state of Fe^{2+}. The satellite peaks were observed for each Fe2p core-levels. In the Mn2p spectrum of pristine NFMO (Fig. S2(c)), two major peaks were observed

at 642.6 and 654 eV, which correspond to $Mn2p_{3/2}$ and $Mn2p_{1/2}$, respectively. Fig. 3(d) reveals that Mn2p peaks are shifted to lower energies, indicating the Li-ion substitution into NFMO causes a
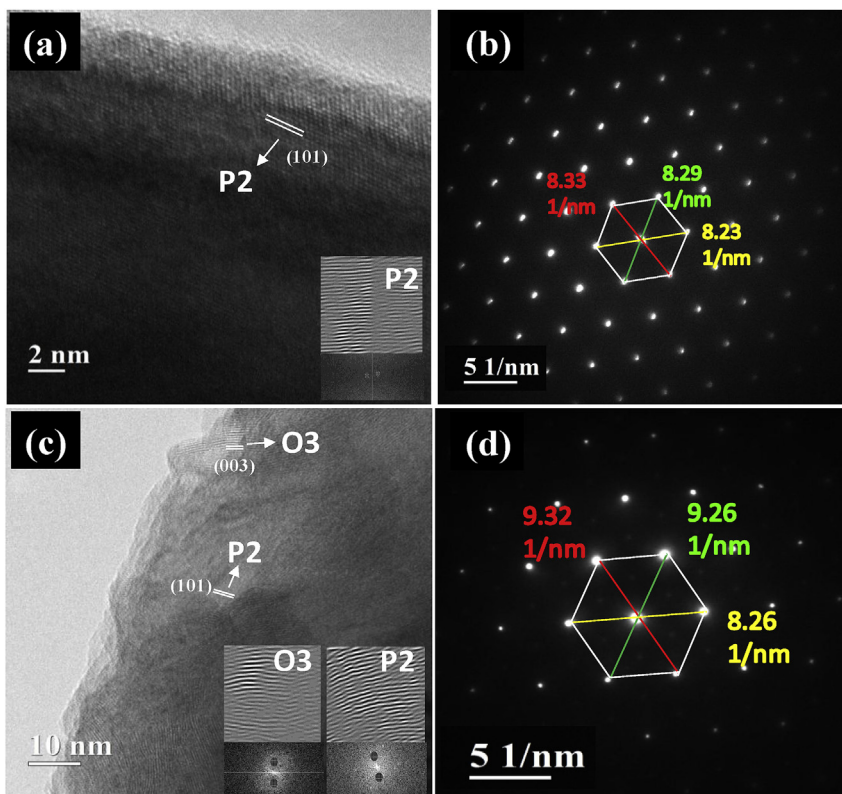

Fig. 4. (a) HR-TEM image and (b) SAED pattern of pristine NFMO. (c) HR-TEM image and (d) SAED pattern of LNFMO-10. Insets in (a) and (c) are FFT images of corresponding lattice fringes.

slight change in oxidation state of Mn from Mn^{3+} to Mn^{4+} [26,41,42]. These XPS results suggest that the substitution of Li-ion into NFMO changes the valence state of Mn rather than that of Fe, which is closely related to the discharge capacity of the samples [43].

The FE-SEM images of the prepared materials are presented in Fig. S3 at same magnification. As can be seen from the figures, the pristine NFMO shows the particle like structure with several μm in particle size. When Li substitutes into NFMO, it does not make any significant changes in the morphology and size of the particles. Fig. 4(a) presents the HR-TEM image of pristine NFMO. The calculated interlayer distance (0.248 nm) is in good agreement with the (101) plane of P2 NFMO. The corresponding SAED pattern in Fig. 4(b) shows an equal distance of 8.28 1/nm in the hexagonal bright spots for NFMO. In case of LNFMO-10, a similar structure was observed in Fig. 4(c). HR-TEM image of LNFMO-10 confirms the presence of P2 and O3 phases. Along with the (101) plane of P2 phase, one more plane was observed in the interlayer distance of 0.54 nm, which can be assigned to the (003) plane for O3 phase (0.55 nm), which indicates the formation of O3 phase by Li-ion substitution. The stacking of these two structures demonstrates the topotactic intergrowth at atomic level, which is consistent with the previous reports [27,32]. In the SAED pattern of LNFMO-10 (Fig. 4(d)), the hexagonal bright spots are observed about 9.29 1/nm in distance (green and red) and distance of 8.26 1/nm (yellow). These results suggest that the substitution of lithium into NFMO widens the interlayer spacing of the P2 phase but slightly tighten that of the O3 phase, which limits the sodium ion diffusion.

However, the presence of O3 in the P2 phase acts as a sodium ion reservoir when combined with the P2, which improves the electrochemical performance [28].

Electrochemical characteristics of the pristine NFMO and LNFMO-n electrodes were investigated by cyclic voltammetry (CV). Fig. 5 shows the CV curves of various electrodes in the voltage range of 1.5–4.0 V at 0.1 mV s^{-1}. The pristine NFMO electrode exhibits two oxidation peaks at 2.57 and 3.80 V, which correspond to the Mn^{3+}/Mn^{4+} and Fe^{3+}/Fe^{4+} reactions, respectively. When introducing the Li content to 0.05 into NFMO, the oxidation state of Mn increases to maintain the charge neutrality, however, there is no change in the oxidation state of Fe. Fig. 5 (b) shows that the peak current for Mn^{3+}/Mn^{4+} is reduced and Fe^{3+}/Fe^{4+} is greatly increased. A small peak shift is observed as compared to pristine NFMO, which is mainly caused by electrode polarization [39]. When Li content is increased to 0.10 and 0.20, the redox currents for Fe^{3+}/Fe^{4+} are further increased. The substitution of high amounts of Li into pristine NFMO increases the oxidation state of Mn from Mn^{3+} to Mn^{4+}, which affects the specific capacity of the electrode material. Although the inactive Mn^{4+} may lead to loss of capacity in LNFMO-20, it can improve the cycling stability by stabilizing the crystal structure during the sodiation/de-sodiation process [44,45]. Among the various electrode materials, the LNFMO-10 electrode exhibited the best reversibility.

Fig. 6 shows the charge and discharge curves (after one preconditioning cycle at 10 mA g^{-1}) of the pristine NFMO, LNFMO-5, LNFMO-10 and LNFMO-20 electrodes, respectively, in the voltage range of 1.5–4.0 V at a constant current of 20 mA g^{-1}. The charge
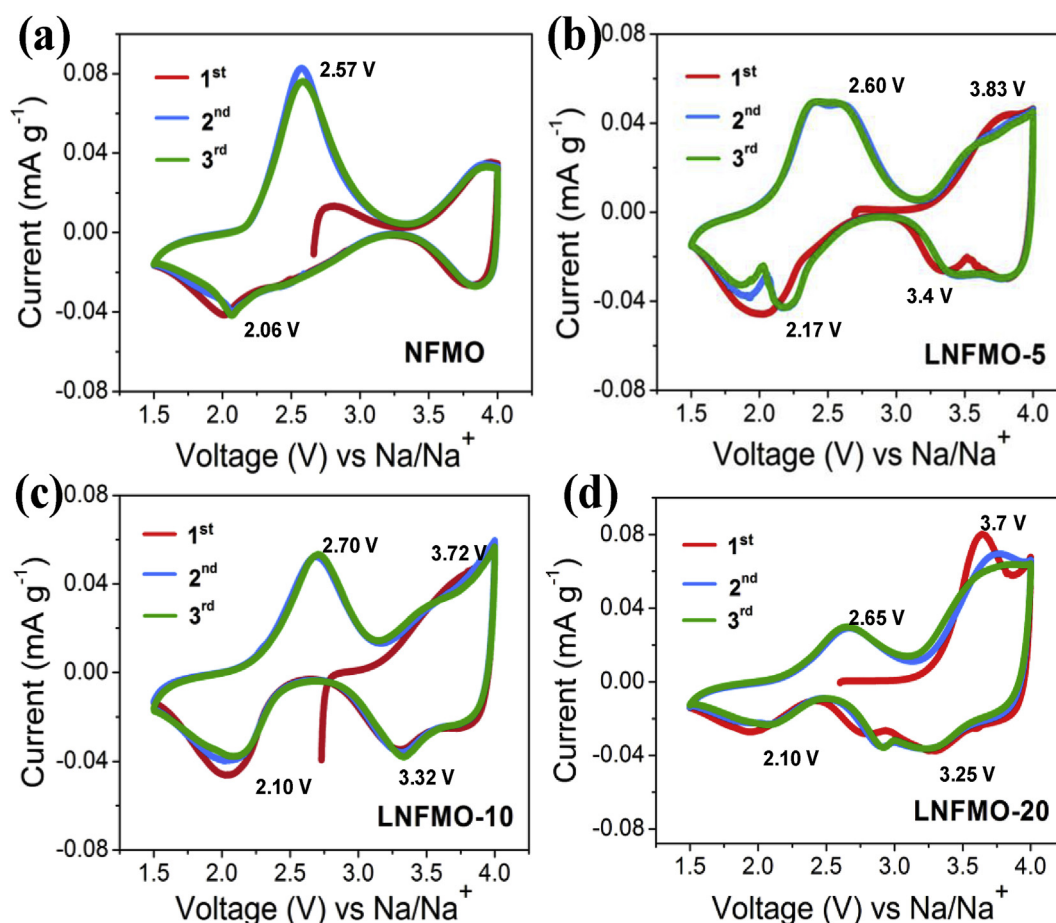

Fig. 5. CV curves of the (a) NFMO, (b) LNFMO-5, (c) LNFMO-10 and (d) LNFMO-20 electrodes at 0.1 mV s^{-1} during three initial cycles.
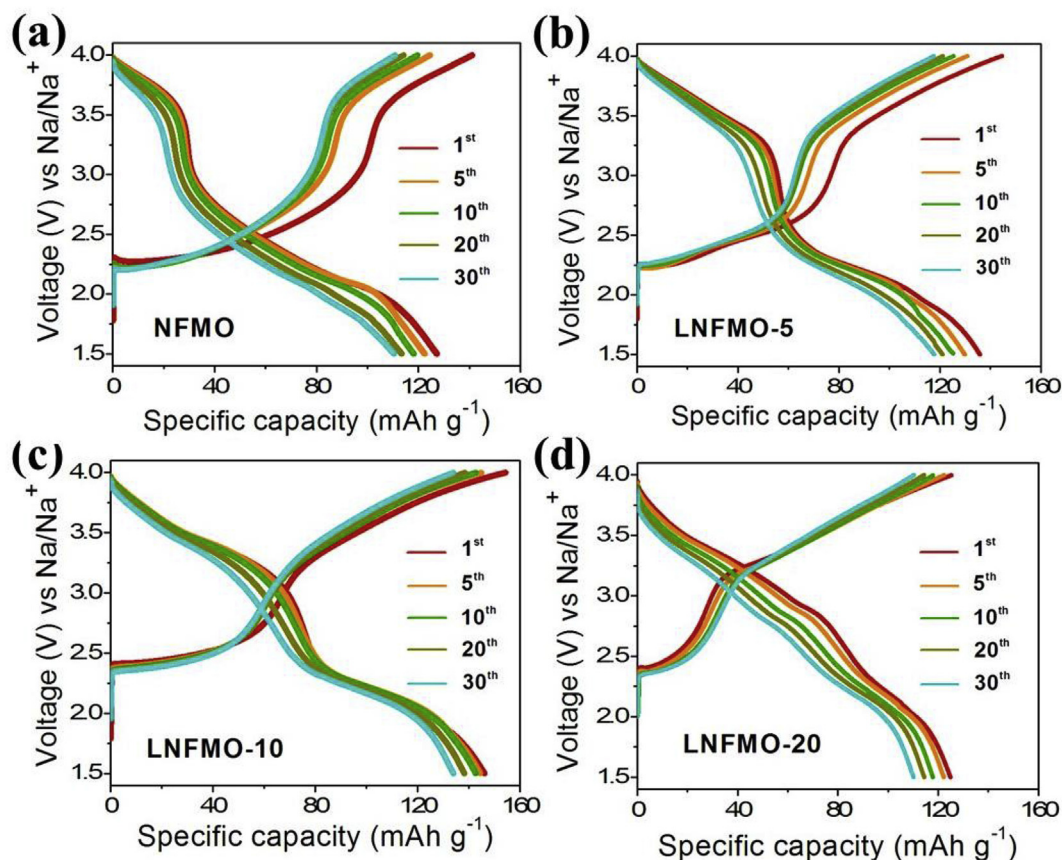
Fig. 6. Charge and discharge curves of (a) NFMO, (b) LNFMO-5, (c) LNFMO-10 and (d) LNFMO-20 electrodes at constant current density of 20 mA g⁻¹.

and discharge curves showed two plateaus around 3.8 and 2.1 V, as previously reported in the literature [42,46,47]. It is found that the average voltage of pristine NFMO was increased from 2.60 to 2.72 V for LNFMO-5, 2.77 V for LNFMO-10 and 2.85 V for LNFMO-20 during the 1st discharge process. Interestingly, the formation of P2+O3 biphasic LNFMO-n by substitution of Li increase the average cell voltage compared to pristine NFMO electrode, which is essential for increasing the energy density of SIBs. It is also found that reversible capacity is increased by substituting Li up to 10 mol% into the pristine NFMO. An initial discharge capacity of 146.2 mAh g⁻¹ was obtained for the LNFMO-10 electrode, which was higher than those of the pristine NFMO and other LNFMO-n electrodes. A decrease of reversible capacity with further increasing the Li content over 10 mol% can be ascribed to the dominance of O3 phase in P2+O3 LNFMO biphase. Fig. S4 shows the charge and discharge curves of the various electrodes at different current densities from 10 to 300 mA g⁻¹. At high current rates, LNFMO-10 electrode shows the highest specific capacity among the electrode materials investigated.

Fig. 7(a) presents the cycling performance of the NFMO and LNFMO-n electrodes at 20 mA g⁻¹. For pristine NFMO electrode, a capacity retention of 85.4% was obtained, whereas both capacity retention and coulombic efficiency were slightly increased for LNFMO-5. The LNFMO-10 electrode exhibited a capacity retention of 92.5% with improved coulombic efficiency compared to pristine NFMO and LNFMO-5. Over the lithium content of 10 mol%, the dominance of O3 phase is occurred, which causes the decrease in specific capacity even though showing relatively high coulombic efficiency and good stability. The rate capability of the electrodes was evaluated, and the results are shown in Fig. 7(b). The pristine

NFMO delivered a discharge capacity of 143.2 mAh g⁻¹ at 10 mA g⁻¹ and the capacity was drastically dropped to 48.9 mAh g⁻¹ at 300 mA g⁻¹. The addition of Li to 5 mol% increased the discharge capacities at all current densities. It should be noted that the LNFMO-10 electrode exhibited the highest discharge capacities at all the current rates investigated. In the case of LNFMO-20 electrode, even though the initial discharge capacity is low at low current density, the discharge capacity was maintained to 70.8 mAh g⁻¹ at 300 mA g⁻¹. These results suggest that the enhanced rate capability can be achieved by P2 and O3 interface architecture. That is to say, the presence of O3 phase provides enough sodium for the intercalation reaction, and the presence of P2 phase favours the enlargement in layered spacing, which further facilitates the sodium ion diffusion and also elevates the average voltage for achieving the high energy density sodium-ion battery.

4. Conclusions

Layered P2+O3 biphasic LNFMO cathode materials were successfully synthesized via lithium-ion substitution by a facile sol-gel approach, and their electrochemical properties were investigated for sodium-ion battery applications. Among various combinations of P2 and O3 biphase, the LNFMO-10 electrode exhibited the highest discharge capacity of 146.2 mAh g⁻¹ with enhanced rate capability and good reversible behaviour compared to the pristine NFMO and other LNFMO-n materials. The improved capacity with enhanced rate performance could be achieved through the enlargement in the layered spacing by the prismatic P2-sites combining with the abundant sodium reservoir of the O3-sites. There are a plenty of layered cathode materials available to
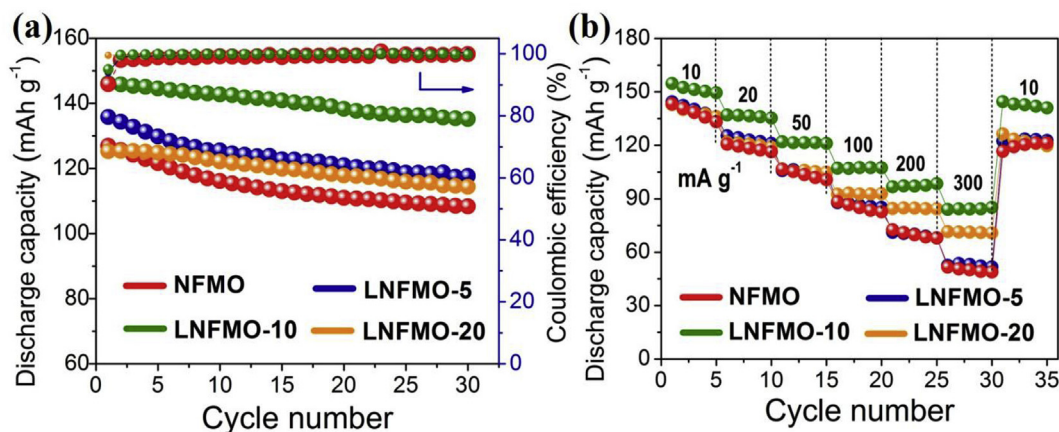
Fig. 7. (a) Cycling performance at 20 mA g^{-1}, and (b) rate capability of the NFMO, LNFMO-5, LNFMO-10 and LNFMO-20 electrodes.

intergrowth with various combinations to create a new avenue for designing novel architecture cathodes with superior electrochemical performance. Hence, the present work will provide a facile and novel strategy for designing high-performance cathode materials for sodium-ion batteries.

Acknowledgements

Appendix A. Supplementary data

Supplementary data to this article can be found online at https://doi.org/10.1016/j.electacta.2018.11.160.

References

[1] L. Schlapbach, A. Zuttel, Hydrogen-storage materials for mobile applications, Nature 414 (2001) 353.
[2] J.B. Goodenough, Y. Kim, Challenges for rechargeable Li batteries, Chem. Mater. 22 (2010) 587.
[3] K.A. Jarvis, C.-C. Wang, J.C. Knight, L. Rabenberg, A. Manthiram, P.J. Ferreira, Formation and effect of orientation domains in layered oxide cathodes of lithium-ion batteries, Acta Mater. 108 (2016) 264.
[4] K. Saravanan, P. Balaya, M.V. Reddy, B.V.R. Chowdari, J.J. Vittal, Morphology controlled synthesis of LiFePO$_4$/C nanoplates for Li-ion batteries, Energy Environ. Sci. 3 (2010) 457.
[5] P.G. Bruce, B. Scrosati, J.M. Tarascon, Nanomaterials for rechargeable lithium batteries, Angew. Chem. Int. Ed. 47 (2008) 2930.
[6] N. Yabuuchi, K. Kubota, M. Dahbi, S. Komaba, Research development on sodium-ion batteries, Chem. Rev. 114 (2014) 11636.
[7] S.W. Kim, D.H. Seo, X. Ma, G. Ceder, K. Kang, Electrode materials for rechargeable sodium-ion batteries: potential alternatives to current lithium-ion batteries, Adv. Energy Mater. 21 (2012) 710.
[8] Y. Lia, Y. Lu, C. Zhao, Y.S. Hu, M.M. Titirici, H. Li, X. Huang, L. Chen, Recent advances of electrode materials for low-cost sodium-ion batteries towards practical application for grid energy storage, Energy Storage Mater. 7 (2017) 130.
[9] N.O. Vitoriano, N.E. Drewett, E. Gonzalo, T. Rojo, High performance manganese-based layered oxide cathodes: overcoming the challenges of sodium ion batteries, Energy Environ. Sci. 10 (2017) 1051.
[10] V. Palomares, P. Serras, I. Villaluenga, K.B. Hueso, J.C. González, T. Rojo, Na-ion batteries, recent advances and present challenges to become low cost energy storage systems, Energy Environ. Sci. 5 (2012) 5884.
[11] L.G. Chagas, D. Buchholz, C. Vaalma, L. Wu, S. Passerini, P-type Na$_x$Ni$_{0.22}$Co$_{0.1}$Mn$_{0.66}$O$_2$ materials: linking synthesis with structure and electrochemical performance, J. Mater. Chem. A 2 (2014) 20263.
[12] R. Berthelot, D. Carlier, C. Delmas, Electrochemical investigation of the P2–Na$_x$CoO$_2$ phase diagram, Nat. Mater. 10 (2011) 74.
[13] N. Yabuuchi, M. Kajiyama, J. Iwatate, H. Nishikawa, S. Hitomi, R. Okuyama, R. Usui, Y. Yamada, S. Komaba, P2-type Na$_x$[Fe$_{1/2}$Mn$_{1/2}$]O$_2$ made from earth-abundant elements for rechargeable Na batteries, Nat. Mater. 11 (2012) 512.
[14] D. Hamani, M. Ati, J.M. Tarascon, P. Rozier, Na$_x$VO$_2$ as possible electrode for Na-ion batteries, Electrochem. Commun. 13 (2011) 938.
[15] H. Xie, C. Wang, S. Tao, G. Wu, Y. Zhou, C. Wu, X. Wang, Y. Sang, L. Song, G. Zhang, G. Pan, A. Marcelli, W. Chu, S. Wei, Ball-in-ball hierarchical design of P2-type layered oxide as high performance Na-ion battery cathodes, Electrochim. Acta 265 (2018) 284.
[16] S.P. Ong, V.L. Chevrier, G. Hautier, A. Jain, C. Moore, S. Kim, X. Ma, G. Ceder, Voltage, stability and diffusion barrier differences between sodium-ion and lithium-ion intercalation materials, Energy Environ. Sci. 4 (2011) 3680.
[17] H.V. Ramasamy, K. Kaliyappan, R. Thangavel, W.M. Seong, K. Kang, Z. Chen, Y.S. Lee, Efficient method of designing stable layered cathode material for sodium ion batteries Using Aluminum Doping, J. Phys. Chem. Lett. 8 (2017) 5021.
[18] H. Wang, B. Yang, X.Z. Liao, J. Xu, D. Yang, Y.S. He, Z.F. Ma, Electrochemical properties of P2-Na$_{2/3}$[Ni$_{1/3}$Mn$_{2/3}$]O$_2$ cathode material for sodium ion batteries when cycled in different voltage ranges, Electrochim. Acta 113 (2013) 200.
[19] L.W. Shacklette, T.R. Jow, L. Townsend, Rechargeable electrodes from sodium cobalt bronzes, J. Electrochem. Soc. 135 (1988) 2669.
[20] A. Caballero, L. Hernan, J. Moralas, L. Sanchez, J. Santos Pena, M.A.G. Aranda, Synthesis and characterization of high-temperature hexagonal P2-Na$_{0.6}$MnO$_2$ and its electrochemical behaviour as cathode in sodium cells, J. Mater. Chem. 12 (2002) 1142.
[21] B. Mortemard de Boisse, D. Carlier, M. Guignard, L. Bourgeois, C. Delmas, P2-Na$_x$Mn$_{1/2}$Fe$_{1/2}$O$_2$ phase used as positive electrode in Na batteries: structural changes induced by the electrochemical (de)intercalation process, Inorg. Chem. 53 (2014) 11197.
[22] B. Mortemard de Boisse, D. Carlier, M. Guignard, C. Delmas, Structural and electrochemical characterizations of P2 and new O3-Na$_x$Mn$_{1-y}$Fe$_y$O$_2$ phases prepared by auto-combustion synthesis for Na-ion batteries, J. Electrochem. Soc. 160 (2013) A569.
[23] Y. Wang, D.D. Yuan, Z. Chen, J. Qian, X. Ai, Y. Cao, H. Yang, Effect of Li$_{1/3}$Mn$_{2/3}$-substitution on electrochemical performance of P2-Na$_{0.74}$CoO$_2$ cathode for sodium-ion batteries, Electrochim. Acta 222 (2016) 862.
[24] C. Fouassier, C. Delmas, P. Hagenmuller, Evolution structurale et proprieties physiques des phases A$_x$MO$_2$ (A = Na. K; M = Cr, Mn, Co) (x ~ i), Mater. Res. Bull. 10 (1975) 443.
[25] M. Sathya, K. Hemalatha, K. Ramesha, J.M. Tarascon, A.S. Prakash, Synthesis, structure, and electrochemical properties of the layered sodium insertion cathode material: NaNi$_{1/3}$Mn$_{1/3}$Co$_{1/3}$O$_2$, Chem. Mater. 24 (2012) 1846.
[26] S.M. Oh, S.T. Myung, J.Y. Hwang, B. Scrosati, K. Amine, Y.K. Sun, High capacity O3-Type Na[Li$_{0.05}$(Ni$_{0.25}$Fe$_{0.25}$Mn$_{0.5}$)$_{0.95}$]O$_2$ cathode for sodium ion batteries, Chem. Mater. 26 (2014) 6165.
[27] E. Lee, J. Lu, Y. Ren, X. Luo, X. Zhang, J. Wen, D. Miller, A. DeWhal, S. Hackney, B. Key, D. Kim, M. Slater, Layered P2-O3 intergrowth cathode: toward high power Na-ion batteries, Adv. Energy. Mater. 4 (2014), 1400458.
[28] S. Guo, P. Liu, H. Yu, Y. Zhu, M. Chen, M. Ishida, H. Zhou, A layered P2- and O3-type composite as a high-energy cathode for rechargeable sodium-ion batteries, Angew. Chem. Int. Ed. 54 (2015) 5894.
[29] M. Keller, D. Buchholz, S. Passerini, Layered Na-ion cathodes with outstanding performance resulting from the synergetic effect of mixed P- and O-Type phases, Adv. Energy Mater. 6 (2016), 1501555.
[30] Z.Y. Li, J. Zhang, R. Gao, H. Zhang, L. Zheng, Z. Hu, X. Liu, Li-Substituted Co-free layered P2/O3 biphasic Na$_{0.67}$Mn$_{0.55}$Ni$_{0.25}$Ti$_{0.2-x}$Li$_x$O$_2$ as high-rate-capability cathode materials for sodium ion batteries, J. Phys. Chem. C 120 (2016) 9007.
[31] G.L. Xu, R. Amine, Y.F. Xu, J. Liu, J. Gim, T. Ma, Y. Ren, C.J. Sun, Y. Liu, X. Zhang,

S. Heald, A. Solhy, I. Saadoune, W.L. Mattis, S.G. Sun, Z. Chen, K. Amine, Insights into the structural effects of layered cathode materials for high voltage sodium-ion batteries, Energy Environ. Sci. 10 (2017) 1677.

[32] X. Qi, L. Liu, N. Song, F. Gao, K. Yang, Y. Lu, H. Yang, Y.S. Hu, Z.H. Cheng, L. Chen, Design and comparative study of O3/P2 hybrid structures for room temperature sodium-ion batteries, ACS Appl. Mater. Interfaces 9 (2017) 40215.

[33] M.S. Kwon, S.G. Lim, Y. Park, S.M. Lee, K.Y. Chung, T.J. Shin, K.T. Lee, P2 orthorhombic $Na_{0.7}[Mn_{1-x}Li_x]O_{2+y}$ as cathode materials for Na-ion batteries, ACS Appl. Mater. Interfaces 9 (2017) 14758.

[34] A.E. Danks, S.R. Hall, Z. Schnepp, The evolution of 'sol–gel' chemistry as a technique for materials synthesis, Mater. Horiz. 3 (2016) 91.

[35] J.Y. Li, H.Y. Lü, X.H. Zhang, Y.M. Xing, G. Wang, H.Y. Guan, X.L. Wu, P2-type $Na_{0.53}MnO_2$ nanorods with superior rate capabilities as advanced cathode material for sodium ion batteries, Chem. Eng. J. 316 (2017) 499.

[36] M.J. Uddin, P.K. Alaboina, S.J. Cho, Nanostructured cathode materials synthesis for lithium-ion batteries, Mater. Today Energy 5 (2017) 138.

[37] M. Pohl, H. Kurig, I. Tallo, A. Jänes, E. Lust, Novel sol-gel synthesis route of carbide-derived carbon composites for very high power density supercapacitors, Chem. Eng. J. 320 (2017) 576.

[38] J. Xu, D.H. Lee, R.J. Clement, X. Yu, M. Leskes, A.J. Pell, G. Pintacuda, X.Q. Yang, C.P. Grey, Y.S. Meng, Identifying the critical role of Li substitution in P2– $Na_x[Li_yNi_zMn_{1-y-z}]O_2$ (0 < x, y, z < 1) intercalation cathode materials for high-energy Na-ion batteries, Chem. Mater. 26 (2014) 1260.

[39] J. Xu, S.L. Chou, J.L. Wang, H.K. Liu, S.X. Dou, Layered P2-$Na_{0.66}Fe_{0.5}Mn_{0.5}O_2$ cathode material for rechargeable sodium-ion batteries, ChemElectroChem 1 (2014) 371.

[40] X. Qi, Y. Wang, L. Jiang, L. Mu, C. Zhao, L. Liu, Y.S. Hu, L. Chen, X. Huang, Sodium-deficient O3-$Na_{0.9}[Ni_{0.4}Mn_xTi_{0.6-x}]O_2$ layered-oxide cathode materials for sodium-ion batteries, Part. Part. Syst. Char. 33 (2016) 538.

[41] Y.E. Zhu, X. Qi, X. Chen, X. Zhou, X. Zhang, J. Wei, Y. Hu, Z. Zhou, A P2-$Na_{0.67}Co_{0.5}Mn_{0.5}O_2$ cathode material with excellent rate capability and cycling stability for sodium-ion batteries, J. Mater. Chem. A 4 (2016) 11103.

[42] P. Manikandan, S. Heo, H.W. Kim, H.Y. Jeong, E. Lee, Y. Kim, Structural characterization of layered $Na_{0.5}Co_{0.5}Mn_{0.5}O_2$ material as a promising cathode for sodium-ion batteries, J. Power Sources 363 (2017) 442.

[43] J. Park, G. Park, H.H. Kwak, S.-T. Hong, J. Lee, Enhanced rate capability and cycle performance of titanium substituted P2-Type $Na_{0.67}Fe_{0.5}Mn_{0.5}O_2$ as a cathode for sodium-ion batteries, ACS Omega 3 (2018) 361.

[44] P.F. Wang, H.R. Yao, X.Y. Liu, J.N. Zhang, L. Gu, X.Q. Yu, Y.X. Yin, Y.G. Guo, Ti-substituted $NaNi_{0.5}Mn_{0.5-x}Ti_xO_2$ cathodes with reversible O3–P3 phase transition for high-performance sodium-ion batteries, Adv. Mater. 29 (2017), 1700210.

[45] Z. Dai, U. Mani, H.T. Tan, Q. Yan, Advanced cathode materials for sodium-ion batteries: what determines our choices? Small Methods 1 (2017), 1700098.

[46] J.S. Throne, R.A. Dunlap, M.N. Obrovac, Structure and electrochemistry of $Na_xFe_xMn_{1-x}O_2$ ($1.0 \leq x \leq 0.5$) for Na-ion battery positive electrodes, J. Electrochem. Soc. 160 (2013) A361.

[47] S. Kalluri, K.H. Seng, W.K. Pang, Z. Guo, Z. Chen, H.K. Liu, S.X. Dou, Electrospun P2-type $Na_{2/3}(Fe_{1/2}Mn_{1/2})O_2$ hierarchical nanofibers as cathode material for sodium-ion batteries, ACS Appl. Mater. Interfaces 6 (2014) 8953.